Microtubule motors mediate endosomal sorting by maintaining functional domain organization.

Sylvie D. Hunt [1], Anna K. Townley [1], Chris M. Danson [2], Peter J. Cullen [2], and David J. Stephens [1*]

*corresponding author

[1] Cell Biology Laboratories, School of Biochemistry, Medical Sciences Building, University of Bristol, University Walk, BRISTOL, BS8 1TD

Tel: +44 (0)117 331 2173, Fax: +44 (0)117 331 2168

Email: david.stephens@bristol.ac.uk

[2] Henry Wellcome Integrated Signalling Laboratories, School of Biochemistry, University of Bristol, Bristol, UK

Running title: Microtubule motors driving endosome dynamics

Keywords: Microtubule motor, endosome, cargo sorting, tubulation.

Number of words (excl. References): 5655

JCS Advance Online Article. Posted on 5 April 2013

Abstract

Many microtubule motors have been shown to couple to endosomal membranes. These motors include dynein as well as many different kinesin family members. Sorting nexins (SNXs) are central to the organization and function of endosomes. These proteins can actively shape endosomal membranes and couple directly or indirectly to the minus-end microtubule motor dynein. Motor proteins acting on endosomes drive their motility, dictate their morphology and impact on cargo segregation.-We have used well-characterized members of the sorting nexin family to elucidate motor coupling using high resolution light microscopy coupled with depletion of specific microtubule motors. Endosomal domains labelled with sorting nexins 1, 4, and 8 (SNX1, SNX4, SNX8) couple to discrete combinations of dynein and kinesin motors. These specific combinations govern the structure and motility of each SNX-coated membrane as well as the segregation of distinct functional endosomal subdomains. Together our data show that these key features of endosome dynamics are governed by the same set of opposing microtubule motors. Thus, microtubule motors help to define the mosaic layout of endosomes that underpins cargo sorting.

Introduction

The endosomal network is highly dynamic with a constant flux of membrane driving membrane trafficking to multiple destinations. Endocytic cargoes can traffic through several pathways either recycling to the cell surface or via a degradative route to the lysosome. Multiple recycling pathways exist which traverse distinct compartments (Anitei and Hoflack, 2011). These pathways govern a diverse array of essential cellular functions including interpretation and down-regulation growth factor and morphogen signalling, organelle positioning as it relates to metabolic sensing, and the uptake and recycling of nutrient receptors. These pathways are also co-opted by various bacterial and viral pathogens that use these systems to avoid degradation.

Microtubule-based motor proteins are integral to the organization and function of the endosomal system. Many different motors have been implicated in discrete trafficking steps (Soldati and Schliwa, 2006; Hunt and Stephens, 2011). Combinations of opposing motors have been implicated in many of these steps; for example, dynein (Aniento et al., 1993) and kinesin-2 (Brown et al., 2005; Loubery et al., 2008) are implicated in traffic to and at late endosomes whereas early endosome motility involves dynein and kinesin-1 (Loubery et al., 2008). Other pathways have been identified that exploit specific members of the kinesin superfamily such as Rab4-dependent trafficking of the fibroblast growth factor receptor (Hoepfner et al., 2005; Ueno et al., 2011). In several systems kinesin-3 family members have been shown to be important, notably in recycling to the plasma membrane. For example UNC-104/KIF1A in *Dictyostelium* (Soppina et al., 2009), kinesin-73 in *Drosophila* (Huckaba et al., 2011), and kinesin-3 in the filamentous fungus *Ustilago* (Schuster et al., 2011b). Dynein (built around the heavy chain DYNC1H1) is clearly a major player in endocytic function with roles in organelle localization (Burkhardt et al., 1997), vesicle movement (Aniento et al., 1993; Oda et al., 1995), and cargo sorting (Driskell et al., 2007). Conflicting data exist surrounding the composition of the dynein motor that is involved in motility and sorting events at the early endosome. In previous work we showed that steady-state localization of the transferrin-positive endocytic recycling compartment was dependent on dynein that contains light intermediate chain 2 LIC2 (DYNC1LI2) (Palmer et al., 2009b) while others have shown roles for both LIC1 (DYNC1LI1) (Horgan et al., 2010b) and LIC2 (Horgan et al., 2010a). Indeed others have suggested that the two LICs have redundant functions in endomembrane traffic (Tan et al., 2011) despite being mutually exclusive components of dynein motors (Tynan et al., 2000). Localization data implicate LIC1 more than LIC2 in endocytic function (Tan et al., 2011).

Much of the complexity of the endosomal system arises from the functional organization of single organelles into domains (Zerial and McBride, 2001). Elegant work has shown that traffic through the endosomal network occurs via a series of endosomal sub-domains (and ultimately endosomes) coated first with Rab5, then Rab7 and finally Rab11 . These functional units are generated and maintained by their protein contents including members of the Rab and sorting nexin (SNX) families. (Cullen and Korswagen, 2012). Recent data have correlated the SNX-dependent tubulation events with the maturation of the endosomal system (which can be defined by Rab localization) (van Weering et al., 2012a). This work defining SNX1, SNX4, and SNX8 localization relative to Rab5, Rab7, and Rab11, produces a more unified view of endosomal architecture by correlating SNX-dependent tubulation (van Weering et al., 2012a).

While several mechanisms of coupling between molecular motors and endosomal membranes have been defined (Hunt and Stephens, 2011), several of the SNX proteins have been shown to form multi-protein complexes with dynein to couple cargo-enriched tubule subdomains to the microtubule network (van Weering et al., 2010; Hunt and Stephens, 2011). Associations between sorting nexins and motor proteins might help tubulation and / or membrane fission. Given their role of SNX proteins in geometric cargo sorting (van Weering et al., 2010), SNX-motor coupling could also be involved in cargo sorting.

SNX1 is a component of the retromer complex, mediating traffic from early endosomes back to the trans-Golgi network (TGN) (Carlton et al., 2004). The mammalian retromer includes SNX1 or SNX2 in concert with SNX5 or SNX6 (Carlton et al., 2004; Carlton et al., 2005; Wassmer et al., 2007; McGough and Cullen, 2011). SNX5/SNX6 couples to the dynein motor complex through an interaction with $p150^{Glued}$, a subunit of the dynein accessory complex dynactin (Hong et al., 2009; Wassmer et al., 2009). This coupling is required for both the formation and fission of tubular carriers.

SNX4 is involved in the endosomal recycling pathway; it is associated with specific tubular elements which are spatially and functionally different to the SNX1-retromer complex (Traer et al., 2007). Suppression of SNX4 expression leads to a defect on transferrin receptor sorting. SNX4, SNX7 and SNX30 are the mammalian orthologues of the yeast Snx4p, Snx41p and Snx42p complexes involved in the recycling pathway (Hettema et al., 2003). SNX4 has also been reported to interact with amphiphysin-2 (Leprince et al., 2003) and clathrin (Skanland et al., 2009).

SNX8 localizes to early endosome (Dyve et al., 2009) and partially colocalizes with the retromer complex (van Weering et al., 2012a). Its suppression has a direct effect on the retrograde transport

endosome-to-TGN trafficking (Dyve et al., 2009). As a member of the SNX-BAR subfamily it is also capable of generating tubular endosomal carriers. It is understood to function in retromer-independent endosome-to-TGN traffic (van Weering et al., 2012a) making it an interesting comparator to SNX1 in terms of endosome organization and transport. SNX8 regulates endosome-to-TGN transport (Dyve et al., 2009) through a pathway that is distinct from that of the SNX1-containing retromer complex (van Weering et al., 2012b; van Weering et al., 2012a). SNX8 has also been identified as a modifier gene for beta-amyloid toxicity (Rosenthal et al., 2012) with some single nucleotide polymorphisms leading to a greater risk of late onset Alzheimer's disease.

Thus, SNX1, SNX4, and SNX8 provide three markers for the functional organization of endosomes that are each linked to microtubule-based motor function. We chose to study the functional coupling of these SNX-coated membrane domains to different motors in order to answer the following questions. First, does each endosomal subdomain couple to the same motor complexes for motility as for tubulation? Second, does this motor coupling impact directly on domain architecture of endosomes? Third, how does the SNX-dependent tubulation of these membranes relate to the application of force by microtubule motors?

Results

We used small interfering RNAs to suppress expression of specific motor protein subunits using oligonucleotides duplexes that we have previously characterized (Gupta et al., 2008; Palmer et al., 2009b). We selected those subunits for which clear evidence for a role in endosomal motility is evident and which we have validated siRNAs ((Gupta et al., 2008; Palmer et al., 2009a). In addition, we also set out to rationalize conflicting data relating to the role of LIC1 and LIC2 in endosomal sorting. Two independent siRNAs were used in all experiments with indistinguishable outcomes; for clarity the results are shown from one siRNA. Efficacy of depletion was monitored by immunoblotting (Supplementary Figure S1). We coupled this with fluorescence imaging of cells stably or transiently expressing fluorescent protein-tagged SNX proteins (SNX1 and SNX8 were stably expressed, SNX4 transiently expressed) (SNX1, SNX4, or SNX8). In order to obtain better spatial and temporal resolution of endocytic traffic we chose to use hTERT-RPE1 cells (human telomerase immortalized retinal pigment epithelial cells) and total internal reflection fluorescence (TIRF) microscopy. The flat morphology of these cells, coupled with TIRF imaging of only those objects close to the coverslip greatly increases the signal-to-noise ratio of our data facilitating more accurate object localization and tracking. The use of TIRF brings a caveat as only a subset of endosomes can be imaged. However, as shown in Supplementary Figure S3, with the configuration that we used, 70-80% of endosomes were visualized depending on their SNX-coating. On the system used, our chosen penetration depth (150 nm) represents the depth at which 30% of the illumination intensity is lost; many fluorescent-tagged structures are therefore excited and detected beyond that depth. Our rationale was not to use TIRF to image only those events happening beneath the plasma membrane but to improve overall spatial and temporal resolution through enhancing the signal to noise ratio.

Microtubule motor coupling to SNX1, SNX4, and SNX8.

We first sought to test the hypothesis that different trafficking routes from early endosomes can be defined by the cohort of microtubule motors to which they couple. Indeed different kinesins have been linked to specific trafficking routes. Using TIRF imaging and object tracking, we compared motility of endosomes labelled with GFP-SNX1 in cells transfected with control siRNA (Fig. 1A, Movie S1) versus those in which we depleted different microtubule motor subunits: dynein-1 heavy chain (DHC1) Kinesin-1 (KIF5B), kinesin-2 accessory protein (KAP2), dynein light intermediate chains 1&2 (LIC1 & LIC2 respectively). These data are shown in Figure 1B-F and in Supplementary Movies S2-S6). These data revealed key differences in both endosomal structure and dynamics following motor depletion and enabled us to define those subunits that couple to SNX1-coated endosomal domains.

Fig. 1A'-F' show colour coded maximum intensity time projections in which all 300 frames of each sequence are colour coded frame by frame (see Movie S7 for an example of this colour coding over time). This allows simple visualization of organelle dynamics. Immobile objects appear white, those moving rapidly show linear paths of a single colour (where all motility occurs within a few frames), while those moving more slowly appear as multi-coloured tracks. In control cells, GFP-SNX1 labelled endosomes are moving rapidly thus the tracks observed in the colour coded panel are of a single colour (see the green track). These data sets were then quantified (Figure 2) to define the numbers of objects moving long distances (>500 nm), short distances (<500 nm but >200 nm) or that were immobile. Distances were determined by eye and accuracy of this assignment of displacement lengths was checked using 2D Gaussian fitting (Spence et al., 2008). Together, Figures 1 and 2 show that GFP-SNX1 labelled endosomes are driven by dynein-1 containing LIC2 and by kinesin-1. We then repeated this approach using GFP-SNX4 and GFP-SNX8 quantifying the motility of endosomes according to whether they underwent long range motility (>500 nm), short range motility (<500 nm), or were immobile. Figure 2B shows that GFP-SNX4 couples to dynein containing LIC2 and kinesin-2, and Figure 2C shows that GFP-SNX8 labelled endosomes couple to dynein containing LIC1 and kinesin-1. Thus, each endosomal domain couples to a distinct cohort of motors that drive their motility.

Microtubule motors govern endosomal structure.

We also noted that the structure of SNX-coated endosomes was altered following depletion of microtubule motors. Examples of endosomal tubulation on motor depletion are shown in Figure 3A. By analyzing image sequences we quantified the tubulation of these domains by measuring both numbers of tubules per cell as well as their length. We multiplied these parameters to define a "tubulation index" (Fig. 3B) which then facilitates analysis of both parameters, taking into account situations where there might be more but shorted tubules, more but longer and so on. These data are presented in Fig. 3C-E. Fig. 3C shows the proportion of tubules in each case, Fig 3D shows the length of tubules, and Fig. 3E the tubulation index which we have colour coded as indicated. These data show that the outcome with respect to tubulation exactly mirrors that of motility (Figure 1). The depletion of specific microtubule motor subunits impairing both motility and architecture (tubulation) suggests a robust functional coupling of these motors to these endosomal domains.

Live cell imaging showed that depletion of motors completely abolished tension induced membrane fission seen occasionally in control cells. Supplementary Movie S8 illustrates longitudinal tension for scission as has been shown by others (Hong et al., 2009). These events were never seen in cells

depleted of motor subunits that drive motility of the domain under investigation. Neither nocodazole nor cytochalasin D treatment of motor-depleted cells reduced the number of tubules seen following motor depletion suggesting that neither an intact microtubule network nor actin filaments are required to maintain the persistence of these tubules.

Motor-dependent organization of endosomes.

SNX1, SNX4, and SNX8 segregate into distinct functional domains thereby defining distinct SNX-motor dependent pathways (van Weering et al., 2010). We sought to determine whether the differential motor coupling that we see when analysing motility and tubulation also has functional outcomes with regard to generation of these distinct domains. This would indicate that motor coupling directs these different sorting pathways from the same early endosomal network as has been suggested by others (Driskell et al., 2007). We therefore determined the level of colocalization of each sorting nexin with the two others when co-expressed in the same cell, for example, the degree of colocalization between mCherry-SNX1 and GFP-SNX4 and between mCherry-SNX1 and GFP-SNX8 and so on. TIRF imaging showed that depletion of microtubule motors subunits caused a significant increase in colocalization of these sorting nexins consistent with a failure to generate or maintain endosomal domain structure. Our analysis used a reference channel (e.g. GFP-SNX4) and asked how many of these structures were also positive for mCherry-SNX1 (Figure 4A). We find that dynein-1 containing LIC2 and kinesin-1 are coupled to mCherry-SNX1-positive domains (Figure 4A and B), dynein-1 containing LIC2 and kinesin-2 are coupled to GFP-SNX4-positive domains, and dynein-1 containing LIC1 and kinesin-1 are coupled to mCherry-SNX8-positive endosomal domains. These data precisely phenocopy the outcomes of motility and tubulation assays. From these data, we conclude that the same cohort of motors is used to drive tubulation and motility and that these features also link to segregation of functional domains.

Discussion

Our data show that coupling of microtubule motors to endosomal membranes is required to maintain the identity of discrete functional domains. Here, we have defined these functional domains using sorting nexins that direct sorting of discrete cargoes along specific pathways (van Weering et al., 2010; van Weering et al., 2012a). Previous work has shown that dynein is required for correct endosomal sorting of transferrin and epidermal growth factor receptors (Driskell et al., 2007). Our data suggest that this is mediated through the generation and/or maintenance of discrete sorting domains for recycling versus degradation. In support of this, previous work has shown that SNX4 and SNX1 direct cargo down different routes (Traer et al., 2007; Wassmer et al., 2009). More recent work demonstrates the molecular interactions that underpin this selective association of SNX family members to generate discrete tubules from a single endosome (van Weering et al., 2012b; van Weering et al., 2012a). In addition, our data define the cohort of motors that mediate this functional domain organization. Perhaps surprisingly, we find that it is the same cohort of motors that direct this domain organization that mediate motility of these SNX-labelled endosomes. We define dynein-1 and kinesin-1 as motors for SNX1- and SNX8-labelled membranes and dynein-1 and kinesin-2 as motors for SNX4-labelled endosomes. All of these motors have been shown previously to mediate endosomal functions in many systems (Aniento et al., 1993; Brown et al., 2005; Nath et al., 2007; Schuster et al., 2011a). Our data highlight a specificity of motor coupling with respect to domain organization and motility of early endosomes. Given the number of microtubule motor subunits encoded in the human genome, other motors are certainly involved in these processes, for example KIF16B which cooperates with Rab14 (Ueno et al., 2011),

In our experiments, depletion of any one motor appears to effectively inhibit all long range translocation. This is consistent with the notion that pairs of opposing motors are required to initiate and sustain long range motility of organelles (Ally et al., 2009). Gelfand and colleagues showed this to be true for peroxisomes in *Drosophila* cells and here we demonstrate the same principle for endosomes in human cells. However, it is important to note that this phenomenon is not necessarily universal and indeed other systems might reply on a single motor species for directed long range motility. This certainly seems to be the case for motility of the endoplasmic reticulum (Wozniak et al., 2009).

The recruitment of dynein to endosomes has been shown to be mediated by the LIC subunits of the motor (Tan et al., 2011). Indeed using isoform specific antibodies, this work suggested a greater localization of LIC1 to early endosomes compared to LIC2. Our own previous work found that LIC2

but not LIC1 was required for transferrin-positive endosomal function (Palmer et al., 2009b). Others have reported redundant functions for both LICs ((Tan et al., 2011) and C. Villemant, A. Mironov, N. Flores-Rodriguez, P.G. Woodman and V.J. Allan, Personal communication, referenced in (Allan, 2011)). LIC1 and LIC2 are mutually exclusive components of dynein motors and so define distinct motors (Tynan et al., 2000). The data we present here go some way to reconciling these discrepancies. As we have shown previously, LIC2 is the predominant form of dynein that couples to the SNX4-transferrin recycling route (Traer et al., 2007; Palmer et al., 2009b). Our data also support that this is the predominant form of dynein on the SNX1-retromer pathway from the early endosome to the trans-Golgi network (TGN) (Wassmer et al., 2009). This led to our conclusion that LIC2-dynein predominated in endosomal sorting. Our current data however suggest that LIC1 containing dynein also has a significant role at early endosomes but on a SNX8-dependent pathway.

The precise function and pathways directed by SNX8 remain unclear but it is suggested to act in a parallel pathway from endosomes to TGN to SNX1 (Dyve et al., 2009). SNX8 homodimers have very little affinity for SNX1/SNX5 and form distinct domains (van Weering et al., 2012b). Although like SNX1 and SNX4, SNX8 is targeted to the early endosome, these three sorting nexins direct separate endosomal sorting events and define distinct membrane trafficking pathways (van Weering et al., 2012b; van Weering et al., 2012a).

Following depletion of motors from cells, we observe a significant increase in tubulation of endosomes. In time lapse imaging we observe few and short tubules at steady state. While increased expression of the chosen SNXs could drive membrane tubulation, control cells are not displaying a significantly high level of tubulation. Moreover, all counting was done against control cells expressing our proteins of interest using the same expression systems. We do occasionally observe tubules emanating from a larger structure in control cells that ultimately release a budding structure from the end (Supplementary Figure S2 and Movie S8). These fission events are not seen in cells depleted of the motor subunits that drive motility of the relevant endosomal domains. Consistent with other previous work (Hong et al., 2009; Wassmer et al., 2009), we interpret this as meaning that microtubule motors apply a longitudinal force to these tubules to facilitate scission. On perturbation of motor coupling, increased tubulation could result from a failure to drive fission through this mechanism.

In our hands, an intact microtubule network is not required to maintain these tubules once formed. We make a distinction here between other data which has investigated the role of microtubules in formation of the SNX-coated tubules (e.g. (Kerr et al., 2006)) versus our experiments which really

only address the role of microtubules in their maintenance. These tubules are notoriously difficult to retain on fixation making interpretation complex. Our data are consistent with a model where the microtubules are required for the formation of these tubules but without the correct motor activity, they persist, even in the absence of an intact microtubule network. This persistence might be dictated by the self-assembly of SNX proteins into higher order structures on the membrane owing to a lack of tension-induced fission (Carlton et al., 2004; van Weering et al., 2012b). Our experiments do not address the role of an intact microtubule network nor of the motors themselves in generating these tubules. Our data are consistent with models of geometric sorting in which the sorting nexins generate tubular domains into which cargo is segregated (van Weering et al., 2010). The role of the motors here is to drive scission to ensure vectorial transport.

In summary, our data show that a defined cohort of microtubule motors are recruited to individual subdomains of the endosomal network where they drive motility, vectorial transport, and participate in the maintenance of the functional architecture of these organelles. A key outcome of our data is that it is the same set of motors that defines each of these events at any one endosomal domain.

Materials and Methods

All reagents were purchased from Sigma-Aldrich (Poole, UK) unless otherwise stated. Small interfering RNAs were used to suppress the expression of specific motors. Two independent siRNAs were used in all experiments with indistinguishable outcomes; for clarity the results are shown from one siRNA. Efficacy of depletion was monitored by immunoblotting (Supplementary Figure S1). SNX1 and SNX8 were stably expressed with a lentiviral expression system and SNX4 transiently expressed in cells from a plasmid. In order to obtain better spatial and temporal resolution of endocytic traffic we chose to use hTERT-RPE1 cells (human telomerase immortalized retinal pigment epithelial cells) and total internal reflection fluorescence (TIRF) microscopy. The flat morphology of these cells, coupled with TIRF imaging of only those objects close to the coverslip greatly increases the signal-to-noise ratio of our data facilitating more accurate object localization and tracking.

Growth of culture cells

Human telomerase immortalized retinal pigment epithelial cells (hTERT-RPE1) were maintained in DMEM-F12 supplemented with 10% FCS (Invitrogen, Paisley, UK) containing supplemented 1% L-glutamine and 1% essential amino-acids. At 24 hours prior to the start of the experiments, cells were seeded onto 35 mm glass bottom dishes (MatTek, Ashland, MA).

Source of antibodies and other reagents

Monoclonal rat anti-human tubulin (ab6160) and polyclonal rabbit anti-KIF5B (ab5629) were from Abcam (Cambridge); polyclonal rabbit anti-human kinesin-2 (kindly provided by Isabelle Vernos, Barcelona, Spain); anti-human dynein light intermediate chains LIC1 and LIC2 were generously provided by Richard Vallee (Tynan et al., 2000); polyclonal rabbit anti-human lamin A/C (cell signalling 2032) was from Cell Signalling Technology (Danvers, MA); monoclonal mouse anti-γ-tubulin (T6557 clone GTU88) was from Sigma-Aldrich (Poole, UK). Fluorophore-conjugated secondary antibodies were from Jackson ImmunoResearch Laboratories (West Grove, PA).

Small interfering RNA transfection

Cells were siRNA-transfected by calcium phosphate method at 3% CO_2 (Chen and Okayama, 1988). The medium was changed 20 hours after transfection and cells were washed with PBS and were incubated for 72 hours at 37°C at 5% CO_2 with fresh supplemented media. SiRNA duplexes were designed using online algorithms of, and subsequently synthesized by, MWG-Eurofins. BLAST search

was performed for these duplexes against the non-redundant database to determine their specificity. All siRNAs have been described previously in (Gupta et al., 2008) or (Palmer et al., 2009b). Two independent siRNAs were used in all experiments with indistinguishable outcomes; for clarity the results are shown from one siRNA. Lamin A/C or luciferase GL2 were depleted as targeted controls. Sequences used were as follow: DHC1-a ACA UCA ACA UAG ACA UUC ATT; DHC1-b CCA AGC AGA UAA GGC AAU ATT; KIF5B-a UGA AUU GCU UAG UGA UGA ATT; KIF5B-b UCA AGU CAU UGA CUG AAU ATT; KAP3-a CUU GAC CAU UCC AGA CUU ATT; KAP3-b GCU CUG UGU AUG AAU AUU ATT; LIC1-a AGA UGA CAG UGU AGU UGU ATT; LIC1-b GAA CAU GAC UAC AGA GAU GTT; LIC2-a ACC UCG ACU UGU UGU AUA ATT; LIC2-b GCC GGA AGA UGC AUA UGA ATT; Lamin A/C CUG GAC UUC CAG AAG AAC ATT; GL2 CGU ACG CGG AAU ACU UCG AUU TT.

Transient plasmid expression

All FP-SNX plasmids were kindly supplied by Pete Cullen's group (University of Bristol, School of Biochemistry). Transient expression of GFP-SNX1, GFP-SNX4, GFP-SNX8, mCherry-SNX1 and mCherry-SNX4 for motor-dependent endosomal sorting assays was done using Lipofectamine™ 2000 as per manufacturer's instructions. Transient expression of GFP-SNX4 was also used for microtubule motor coupling assay.

Lentiviral construct and generation of stable cell lines

All viruses were kindly supplied by Pete Cullen's group (University of Bristol, School of Biochemistry). Cells were plated at 1.5 x 10^5 cells per 3 cm culture dish and infected with lentivirus particles after 24 h growth; media was replaced by fresh supplemented media after 24 h. Cells were split as usual after an additional 48 h. Following puromycin selection stable cell lines were verified by immunofluorescence. Transduced cells were stably expressing the constructs after 72 h. These GFP-SNX1 and GFP-SNX8 stable cell lines have been used for microtubule motor coupling assays.

Immunolabelling

Medium was removed and cells were subsequently washed with PBS. Cells were then fixed using 4% paraformaldehyde for 20 minutes at room temperature. A solution of glycine (30 mM) in PBS was then added for 5 minutes at room temperature. Cells were thereafter permeabilized with a solution of 0.1% Triton X100 in PBS for 5 minutes at room temperature. After two washes in PBS, cells were blocked using a 3% bovine serum albumin (BSA) in PBS for 30 minutes at room temperature. Cells were incubated with the primary antibodies in 3% BSA for 1 hour at room temperature. Three

washes with PBS of 5 minutes each at room temperature were done before incubating the secondary antibody. The latter was diluted at 1:400 in PBS and incubated 1 hour at room temperature. Finally, after three washes in PBS (5 minutes each at room temperature) and an optional nuclear staining with DAPI (4,6-Diamidino-2-phenylindole, Molecular Probes, diluted at 1:5000 in distilled water) for 3 minutes at room temperature, cells were gently rinsed twice in PBS.

Immunoblotting

For all immunoblots, cells were lysed and samples were separated by SDS-PAGE followed by transfer to nitrocellulose membranes; primary antibodies were detected using HRP-conjugated secondary antibodies (Jackson ImmunoResearch, West Grove, PA) and enhanced chemiluminescence (ECL, GE Healthcare, Cardiff, UK).

Nocodazole treatment

Nocodazole was used at the final concentration of 5 $\mu g.ml^{-1}$ in culture media. After 1 h incubation at 37°C, cells were observed live in imaging media (red-phenol free DMEM, 30 mM HEPES pH 7.4, $NaHCO_3$ 0.05 $g.l^{-1}$) containing nocodazole at the same concentration thus preventing cell recovery from the drug treatment.

Transferrin uptake assay

Cells were washed twice in imaging media (red-phenol free DMEM, 30 mM Hepes pH 7.4, $NaHCO_3$ 0.05$g.l^{-1}$); transferrin-Alexa Fluor 568 (Molecular Probes) was diluted to 100 $\mu g.ml^{-1}$ in imaging media and added to cells. After 15 minutes incubation at 37°C, cells were washed twice in imaging media pre-warmed at 37°C and imaged as usual.

TIRF Imaging

Cells were kept at 37°C and at 5% CO_2. Media was discarded and replaced with pre-warmed imaging media just prior imaging. The TIRF system used was a Leica AM-TIRF MC (multi colour) associated with a Leica DMI 6000 inverted microscope. Images were acquired with an Olympus oil immersion TIRF objective with 100x 1.46 numerical aperture and were acquired at the rate 12.04 frames per second (e.g. interval between pictures set at 83 ms) using a Hamamatsu C9100-13 EMCCD camera. Each image was 512 by 512 pixels with no additional binning. Laser lines available were at 405 nm, 488 nm, 561 nm and 635 nm. Data was processed using Volocity software (Perkin Elmer) and Adobe

Illustrator CS (Adobe). TIRF Imaging was used in all assays. The penetration depth used was set at 150 nm to optimise the ratio signal / noise. For motor-dependent endosomal sorting assays, thousand frames were acquired. Colocalization studies were also performed on live cells to keep the tubular structures intact. Image brightness and contrast was adjusted in ImageJ/Fiji and the same processing was applied to all image sets within each experiment.

Quantification of image data and statistical analysis

After TIRF acquisition, movies were imported in Volocity 5.4.1 (Perkin Elmer). The long range and short range of movement have been typically determined using 2D Gaussian fitting. Due to the large size and pleiomorphic nature of endosomes, the number of vesicles to be tracked and their numerous interferences with the background, counting was done by hand after visual verification of the displacement level. Object tracking was performed manually and distance accuracy was checked using two-dimensional (2D) Gaussian fitting of pixel intensities as described elsewhere (Gupta et al., 2008; Spence et al., 2008). Colour coding of time sequences was achieved using an ImageJ plug-in developed by Kota Miura (EMBL Heidelberg) which is available within the Fiji implementation of ImageJ at: www.fiji.sc (Schindelin et al., 2012). Tubules were counted by hand and their length was determined using the line measurement tool in Volocity 5.4.1 (Perkin Elmer). The proportion of tubules was determined against the number of structures (vesicles and tubules).

Colocalization tools in image analysis software such as Volocity 5.4.1 (Perkin Elmer) or ImageJ (Fiji) give underestimated threshold coefficients due to the partial overlapping of some structures. Thus, in this study colocalized structures were counted by hand. Any overlap of objects was counted as colocalization. Representative images are shown, all experiments were repeated independently at least three times each. Samples were compared using the Mann Whitney test using GraphPad Prism. All images were prepared for publication with Photoshop CS (Adobe)

Acknowledgements

We would like to thank the Wolfson Foundation, MRC, and University of Bristol for establishing and maintaining the University of Bristol Bioimaging Facility and Mark Jepson, Alan Leard for their help with training.

Funding

This work was funded by the UK Medical Research Council (grant number G0801848).

Author contributions

S.D.H. performed the research, analyzed data and contributed to writing the paper, A.K.T. contributed new reagents and analyzed data, C.M.D. contributed new reagents, P.J.C. and D.J.S. designed the research, analyzed data and wrote the paper.

References

Allan, V. J. (2011). Cytoplasmic Dynein. *Biochem. Soc. Trans.* **39**, 1169-1178.

Ally, S., Larson, A. G., Barlan, K., Rice, S. E. and Gelfand, V. I. (2009). Opposite-polarity motors activate one another to trigger cargo transport in live cells. *J. Cell Biol.* **187**, 1071-1082.

Aniento, F., Emans, N., Griffiths, G. and Gruenberg, J. (1993). Cytoplasmic dynein-dependent vesicular transport from early to late endosomes. *J. Cell Biol.* **123**, 1373-1387.

Anitei, M. and Hoflack, B. (2011). Bridging membrane and cytoskeleton dynamics in the secretory and endocytic pathways. *Nat. Cell Biol.* **14**, 11-19.

Brown, C. L., Maier, K. C., Stauber, T., Ginkel, L. M., Wordeman, L., Vernos, I. and Schroer, T. A. (2005). Kinesin-2 is a motor for late endosomes and lysosomes. *Traffic* **6**, 1114-1124.

Burkhardt, J. K., Echeverri, C. J., Nilsson, T. and Vallee, R. B. (1997). Overexpression of the dynamitin (p50) subunit of the dynactin complex disrupts dynein-dependent maintenance of membrane organelle distribution. *J. Cell Biol.* **139**, 469-484.

Carlton, J., Bujny, M., Peter, B. J., Oorschot, V. M., Rutherford, A., Mellor, H., Klumperman, J., McMahon, H. T. and Cullen, P. J. (2004). Sorting nexin-1 mediates tubular endosome-to-TGN transport through coincidence sensing of high- curvature membranes and 3-phosphoinositides. *Current biology* **14**, 1791-1800.

Carlton, J. G., Bujny, M. V., Peter, B. J., Oorschot, V. M., Rutherford, A., Arkell, R. S., Klumperman, J., McMahon, H. T. and Cullen, P. J. (2005). Sorting nexin-2 is associated with tubular elements of the early endosome, but is not essential for retromer-mediated endosome-to-TGN transport. *J. Cell Sci.* **118**, 4527-4539.

Chen, C. A. and Okayama, H. (1988). Calcium phosphate-mediated gene transfer: a highly efficient transfection system for stably transforming cells with plasmid DNA. *BioTechniques* **6**, 632-638.

Cullen, P. J. and Korswagen, H. C. (2012). Sorting nexins provide diversity for retromer-dependent trafficking events. *Nat. Cell Biol.* **14**, 29-37.

Driskell, O. J., Mironov, A., Allan, V. J. and Woodman, P. G. (2007). Dynein is required for receptor sorting and the morphogenesis of early endosomes. *Nat. Cell Biol.* **9**, 113-120.

Dyve, A. B., Bergan, J., Utskarpen, A. and Sandvig, K. (2009). Sorting nexin 8 regulates endosome-to-Golgi transport. *Biochem. Biophys. Res. Commun.* **390**, 109-114.

Elbashir, S. M., Harborth, J., Lendeckel, W., Yalcin, A., Weber, K. and Tuschl, T. (2001). Duplexes of 21-nucleotide RNAs mediate RNA interference in cultured mammalian cells. *Nature* **411**, 494-498.

Gupta, V., Palmer, K. J., Spence, P., Hudson, A. and Stephens, D. J. (2008). Kinesin-1 (uKHC/KIF5B) is required for bidirectional motility of ER exit sites and efficient ER-to-Golgi transport. *Traffic* **9**, 1850-1866.

Hettema, E. H., Lewis, M. J., Black, M. W. and Pelham, H. R. (2003). Retromer and the sorting nexins Snx4/41/42 mediate distinct retrieval pathways from yeast endosomes. *The EMBO journal* **22**, 548-557.

Hoepfner, S., Severin, F., Cabezas, A., Habermann, B., Runge, A., Gillooly, D., Stenmark, H. and Zerial, M. (2005). Modulation of receptor recycling and degradation by the endosomal kinesin KIF16B. *Cell* **121**, 437-450.

Hong, Z., Yang, Y., Zhang, C., Niu, Y., Li, K., Zhao, X. and Liu, J. J. (2009). The retromer component SNX6 interacts with dynactin p150(Glued) and mediates endosome-to-TGN transport. *Cell Research* **19**, 1334-1349.

Horgan, C. P., Hanscom, S. R., Jolly, R. S., Futter, C. E. and McCaffrey, M. W. (2010a). Rab11-FIP3 binds dynein light intermediate chain 2 and its overexpression fragments the Golgi complex. *Biochem. Biophys. Res. Commun.* **394**, 387-392.

Horgan, C. P., Hanscom, S. R., Jolly, R. S., Futter, C. E. and McCaffrey, M. W. (2010b). Rab11-FIP3 links the Rab11 GTPase and cytoplasmic dynein to mediate transport to the endosomal-recycling compartment. *J. Cell Sci.* **123**, 181-191.

Huckaba, T. M., Gennerich, A., Wilhelm, J. E., Chishti, A. H. and Vale, R. D. (2011). Kinesin-73 is a processive motor that localizes to Rab5-containing organelles. *J Biol Chem* **286**, 7457-7467.

Hunt, S. D. and Stephens, D. J. (2011). The role of motor proteins in endosomal sorting. *Biochem. Soc. Trans.* **39**, 1179-1184.

Kerr, M. C., Lindsay, M. R., Luetterforst, R., Hamilton, N., Simpson, F., Parton, R. G., Gleeson, P. A. and Teasdale, R. D. (2006). Visualisation of macropinosome maturation by the recruitment of sorting nexins. *J. Cell Sci.* **119**, 3967-3980.

Leprince, C., Le Scolan, E., Meunier, B., Fraisier, V., Brandon, N., De Gunzburg, J. and Camonis, J. (2003). Sorting nexin 4 and amphiphysin 2, a new partnership between endocytosis and intracellular trafficking. *J. Cell Sci.* **116**, 1937-1948.

Loubery, S., Wilhelm, C., Hurbain, I., Neveu, S., Louvard, D. and Coudrier, E. (2008). Different microtubule motors move early and late endocytic compartments. *Traffic* **9**, 492-509.

McGough, I. J. and Cullen, P. J. (2011). Recent advances in retromer biology. *Traffic* **12**, 963-971.

Nath, S., Bananis, E., Sarkar, S., Stockert, R. J., Sperry, A. O., Murray, J. W. and Wolkoff, A. W. (2007). Kif5B and Kifc1 interact and are required for motility and fission of early endocytic vesicles in mouse liver. *Mol. Biol. Cell* **18**, 1839-1849.

Oda, H., Stockert, R. J., Collins, C., Wang, H., Novikoff, P. M., Satir, P. and Wolkoff, A. W. (1995). Interaction of the microtubule cytoskeleton with endocytic vesicles and cytoplasmic dynein in cultured rat hepatocytes. *J Biol Chem* **270**, 15242-15249.

Palmer, K. J., Hughes, H. and Stephens, D. J. (2009a). Specificity of cytoplasmic dynein subunits in discrete membrane-trafficking steps. *Mol Biol Cell* **20**, 2885-2899.

Palmer, K. J., Hughes, H. and Stephens, D. J. (2009b). Specificity of cytoplasmic dynein subunits in discrete membrane-trafficking steps. *Mol. Biol. Cell* **20**, 2885-2899.

Rosenthal, S. L., Wang, X., Demirci, F. Y., Barmada, M. M., Ganguli, M., Lopez, O. L. and Kamboh, M. I. (2012). Beta-Amyloid Toxicity Modifier Genes and the Risk of Alzheimer's Disease. *Am J Neurodegener Dis* **1**, 191-198.

Schindelin, J., Arganda-Carreras, I., Frise, E., Kaynig, V., Longair, M., Pietzsch, T., Preibisch, S., Rueden, C., Saalfeld, S., Schmid, B. et al. (2012). Fiji: an open-source platform for biological-image analysis. *Nature Methods* **9**, 676-682.

Schuster, M., Lipowsky, R., Assmann, M. A., Lenz, P. and Steinberg, G. (2011a). Transient binding of dynein controls bidirectional long-range motility of early endosomes. *Proc. Natl. Acad. Sci. USA* **108**, 3618-3623.

Schuster, M., Kilaru, S., Fink, G., Collemare, J., Roger, Y. and Steinberg, G. (2011b). Kinesin-3 and dynein cooperate in long-range retrograde endosome motility along a nonuniform microtubule array. *Mol. Biol. Cell* **22**, 3645-3657.

Skanland, S. S., Walchli, S., Brech, A. and Sandvig, K. (2009). SNX4 in complex with clathrin and dynein: implications for endosome movement. *PLoS ONE* **4**, e5935.

Soldati, T. and Schliwa, M. (2006). Powering membrane traffic in endocytosis and recycling. *Nat Rev Mol Cell Biol* **7**, 897-908.

Soppina, V., Rai, A. K., Ramaiya, A. J., Barak, P. and Mallik, R. (2009). Tug-of-war between dissimilar teams of microtubule motors regulates transport and fission of endosomes. *Proc. Natl. Acad. Sci. USA* **106**, 19381-19386.

Spence, P., Gupta, V., Stephens, D. J. and Hudson, A. J. (2008). Optimising the precision for localising fluorescent proteins in living cells by 2D Gaussian fitting of digital images: application to COPII-coated endoplasmic reticulum exit sites. *European biophysics journal : EBJ* **37**, 1335-1349.

Tan, S. C., Scherer, J. and Vallee, R. B. (2011). Recruitment of dynein to late endosomes and lysosomes through light intermediate chains. *Mol. Biol. Cell* **22**, 467-477.

Traer, C. J., Rutherford, A. C., Palmer, K. J., Wassmer, T., Oakley, J., Attar, N., Carlton, J. G., Kremerskothen, J., Stephens, D. J. and Cullen, P. J. (2007). SNX4 coordinates endosomal sorting of TfnR with dynein-mediated transport into the endocytic recycling compartment. *Nat. Cell Biol.* **9**, 1370-1380.

Tynan, S. H., Purohit, A., Doxsey, S. J. and Vallee, R. B. (2000). Light intermediate chain 1 defines a functional subfraction of cytoplasmic dynein which binds to pericentrin. *J Biol Chem* **275**, 32763-32768.

Ueno, H., Huang, X., Tanaka, Y. and Hirokawa, N. (2011). KIF16B/Rab14 molecular motor complex is critical for early embryonic development by transporting FGF receptor. *Dev. Cell* **20**, 60-71.

van Weering, J. R., Verkade, P. and Cullen, P. J. (2010). SNX-BAR proteins in phosphoinositide-mediated, tubular-based endosomal sorting. *Seminars in Cell and Developmental Biology* **21**, 371-380.

van Weering, J. R., Verkade, P. and Cullen, P. J. (2012a). SNX-BAR-mediated endosome tubulation is co-ordinated with endosome maturation. *Traffic* **13**, 94-107.

van Weering, J. R., Sessions, R. B., Traer, C., Kloer, D. P., Bhatia, V. K., Stamou, D., Carlsson, S. R., Hurley, J. H. and Cullen, P. J. (2012b). In vitro SNX-BAR assembly reveals molecular details of distinct endosomal tubule formation. *EMBO J.* **31**, 4466–80.

Wassmer, T., Attar, N., Bujny, M. V., Oakley, J., Traer, C. J. and Cullen, P. J. (2007). A loss-of-function screen reveals SNX5 and SNX6 as potential components of the mammalian retromer. *J. Cell Sci.* **120**, 45-54.

Wassmer, T., Attar, N., Harterink, M., van Weering, J. R., Traer, C. J., Oakley, J., Goud, B., Stephens, D. J., Verkade, P., Korswagen, H. C. et al. (2009). The retromer coat complex coordinates endosomal sorting and dynein-mediated transport, with carrier recognition by the trans-Golgi network. *Dev. Cell* **17**, 110-122.

Wozniak, M. J., Bola, B., Brownhill, K., Yang, Y. C., Levakova, V. and Allan, V. J. (2009). Role of kinesin-1 and cytoplasmic dynein in endoplasmic reticulum movement in Vero cells. *J. Cell Sci.* **122**, 1979-1989.

Zerial, M. and McBride, H. (2001). Rab proteins as membrane organizers. *Nat Rev Mol Cell Biol* **2**, 107-117.

Figure Legends

Figure 1: Microtubule motors driving motility of SNX-labelled endosomal domains.

(A-F) Frames depicting the movement of SNX1-coated endosomes, in control cells (A) and in cells depleted for different microtubule motor subunits (B-F). (A'-F') Colour coded representation of movement: immobile vesicles appear white and moving vesicles appear with coloured tracks. Scale bar is 5 µm on all panels.

Figure 2: Quantification of motility of SNX-labelled endosome domains.

These histograms represent the different subpopulations of SNX decorated structures according to their motility. Long range movements are characterized by a range greater than 500 nm, short range less than 500 nm. The siRNA GL2 targeting the firefly luciferase (Elbashir et al., 2001) was used to transfect control cells throughout this study. When depleted, dynein-1 heavy chain (DHC1, DYNC1H1), kinesin-1 (KIF5), kinesin-2 (KAP3) and dynein light intermediate chains 1&2 (LIC1 and LIC2 resp.) impaired the motility of SNXs. Note GFP-SNX1 endosomes couple to dynein-1 containing LIC2 and kinesin-1, GFP-SNX4 endosomes couple to dynein-1 containing LIC2 and kinesin-2 and GFP-SNX8 endosomes couple to dynein-1 containing LIC1 and kinesin-1. Note that experiments with defined outcomes were repeated 3 times (independently) and error bars are displayed on the subsequent column. Non-effective treatments were repeated twice. This is consistent throughout this study. Asterisks indicate statistical significance from Mann-Whitney test comparing to GL2 controls (*=p<0.05, **=p<0.01, ***=p<0.001).

Figure 3: Tubulation of endosomal domains in the absence of coupled motor proteins.

(A) Highly mobile tubulo-vesicular SNX-decorated structures are moving linearly and bidirectionally in control cells (GL2). Depletion of different motor subunits induced the generation of long tubules (arrows) and enlarged endosomes (asterisks) for SNX1- SNX4- and SNX8-coated endosomes. Scale bar is 5 µm on all panels. (B) This diagram represents the different phenotypes that could be observed in hTERT-RPE1 expressing GFP-tagged SNX. In non treated cells, the percentage of tubules and their length is low as shown in case #1. The two parameters monitored, % tubules and tubule length could be affected by motor depletion as shown in cases #2-#4. A tubulation index (T.I.) is calculated where T.I. = % tubules x length tubule and colour coded for clarity. (C) The proportion of tubules was counted against the number of SNX-labelled structures. (D) The length of tubules in µm has been measured in each case. (E) The tubulation Index is calculated as previously explained and

bar are coloured for greater clarity. A red column indicates case#4 with a high percentage of tubule and a greater length. Mirroring our other data, these results highlight the role of motors in the vesicle scission from endosomes. Asterisks indicate statistical significance from Mann-Whitney test comparing to GL2 controls (*=p<0.05, **=p<0.01, ***=p<0.001).

Figure 4: Microtubule motors direct segregation of endosomes into distinct functional domains.

We determined the colocalization of different SNX proteins following microtubule motor depletion as a measure of functional coupling of motors to these domains. (A) The number of SNX4 labelled structures also labelled with SNX1 is increased following depletion of DHC1, KIF5B, or LIC2. (B) Colocalization of SNX8 and SNX1 following depletion of DHC1, KIF5B, or LIC2. Together A and B indicate that DHC1, KIF5B, or LIC2. Apply force to SNX1-labelled domains. (C, D) The number of (C) SNX1 or (D) SNX8 labelled endosomal domains also labelled with SNX4 is greatly enhanced following depletion of DHC1, KAP3, or LIC2. These data indicate that DHC1, KAP3, and LIC2 apply force to SNX4-positive structures. (E, F) The number of (E) SNX1 or (F) SNX4 labelled endosomal domains also labelled with SNX8 is greatly enhanced following depletion of DHC1, kinesin-1, or LIC1. These data indicate that DHC1, kinesin-1, and LIC1 apply force to SNX8-positive structures. Asterisks indicate statistical significance from Mann-Whitney test comparing to GL2 controls (*=p<0.05, **=p<0.01, ***=p<0.001).

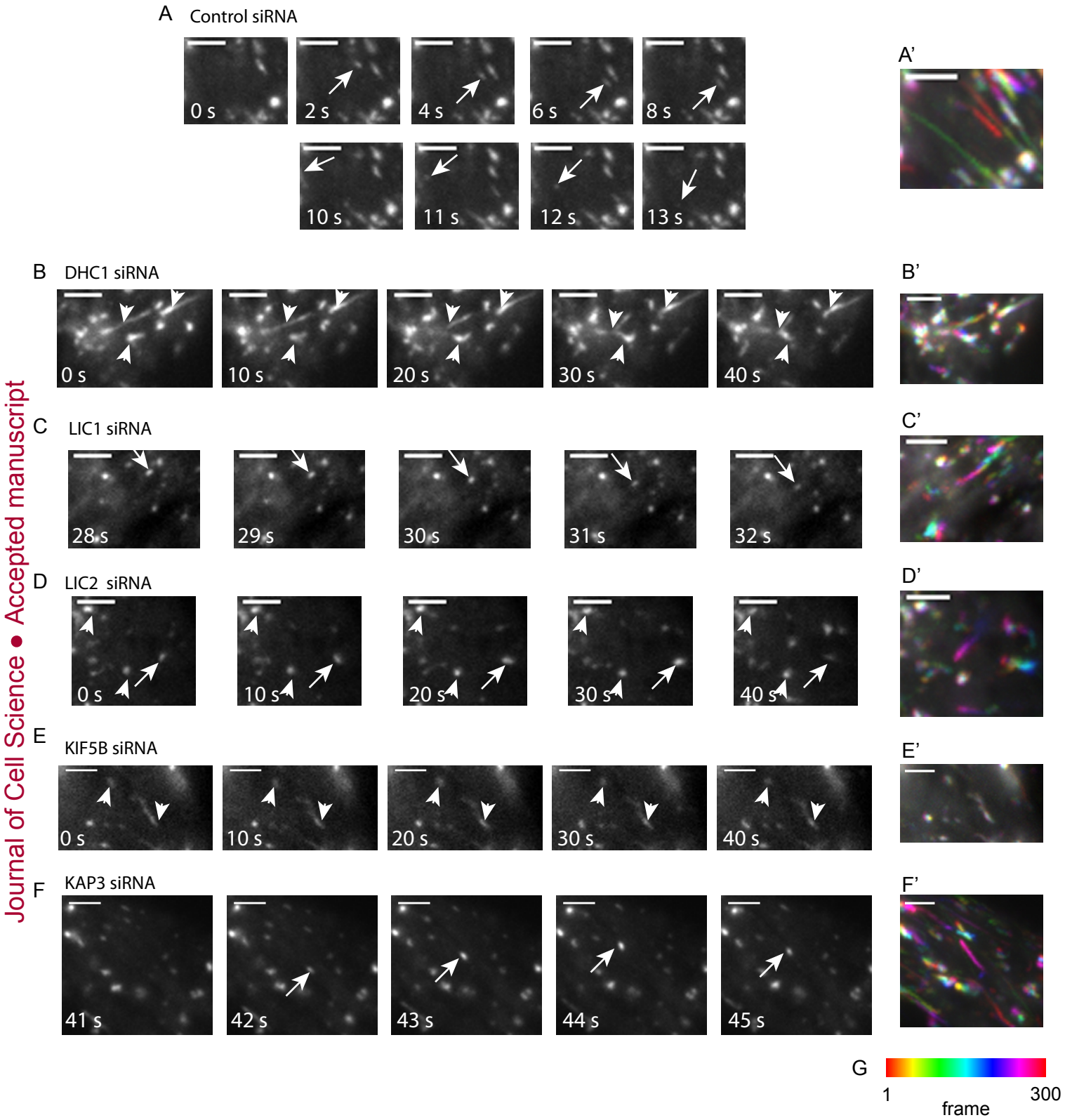

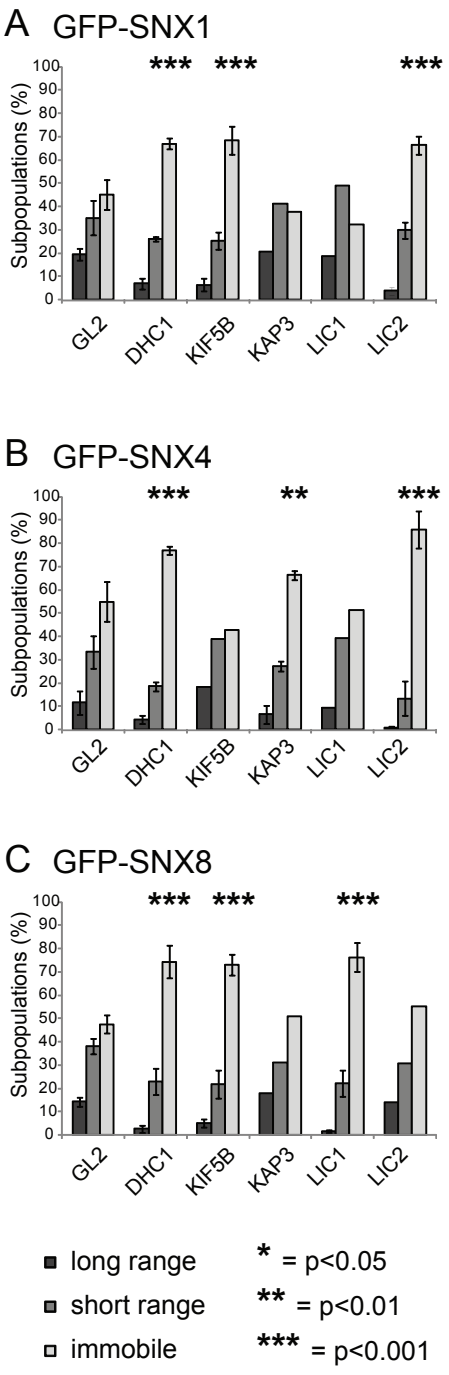

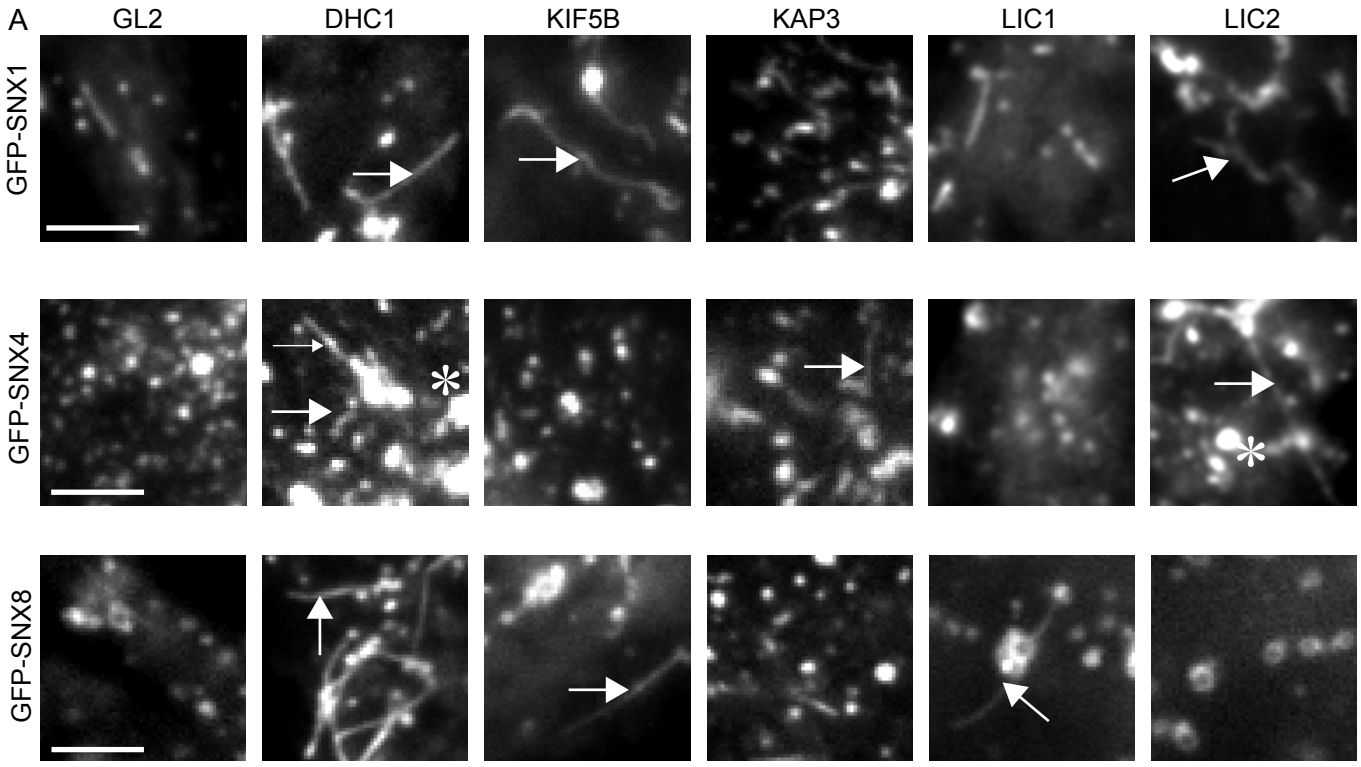

B

Parameter	Case#1	Case#2	Case#3	Case#4
Phenotype	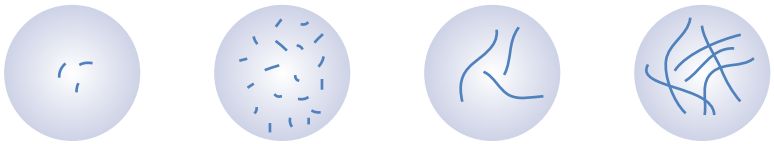			
% tubules	Low	High	Low	High
Length (µm)	Low	Low	High	High
Tubulation Index	Low	Int.1	Int.2	High